

Figure 2. (a, Top) Integral weight CCD, $I_w(x)$, and (b, bottom) differential weight CCD, $W(x)$, for statistical copolymerization of an ordinary monomer A with a macromonomer M for different compositions of the starting mixture of monomers, y_0 , in terms of the weight fraction of monomer A. $r_A = 0.5$; cf. also Figure 1.

(Figure 1). For example, for equal weights of comonomers in the starting mixture (Figure 1), the copolymer prepared up to 50 wt % conversion will contain macromolecules differing by 25 wt % in the content of the macromonomer

for $r_A = 0.1$, 21 wt % for $r_A = 0.2$, 11 wt % for $r_A = 0.5$, and 2 wt % for $r_A = 0.9$ (Figure 1a). At copolymerizations carried out to higher conversion, these differences are still higher (Figure 1a). A figure identical with Figure 1 could be drawn for $r_A = 10, 5, 2$, and 1.1, if x had the meaning of weight fraction of the macromonomer in the copolymer. For low r_A values (e.g., for $r_A = 0.1$ and 0.2 in Figure 1a), the macromonomer is totally depleted from the reaction mixture before complete conversion is reached. A homopolymer from the low molecular weight monomer A is formed in the last stages of polymerization.

The starting composition of the monomer mixture, y_0 , affects the chemical heterogeneity of copolymers in such a way that for $r_A < 1$ the CCD broadens as the weight fraction y_0 of the ordinary monomer A is decreased (Figure 2). The opposite is true for $r_A > 1$.

Conclusions

In copolymers prepared by statistical copolymerization involving a macromonomer, the conversion chemical heterogeneity may be significant. It is expected to be high if the monomer reactivity ratio of the ordinary monomer substantially differs from unity. Such a situation is especially likely to occur when the structure of the macromonomer end group strongly differs from that of the low molecular weight comonomer.⁶

The extent of conversion chemical heterogeneity is independent of molecular weight of the macromonomer and is determined only by the weight fraction of the macromonomer in the starting mixture and by conversion.

References and Notes

- (1) Rempp, P.; Franta, E. *Adv. Polym. Sci.* **1984**, *58*, 1.
- (2) Stockmayer, W. H. *J. Chem. Phys.* **1945**, *13*, 199.
- (3) Stejskal, J.; Kratochvíl, P. *Macromolecules* **1987**, *20*, 2624.
- (4) Meyer, V. E.; Lowry, G. G. *J. Polym. Sci., Part A* **1965**, *3*, 2843.
- (5) Niwa, M.; Hayashi, T.; Akahori, M. *J. Macromol. Sci., Chem.* **1987**, *A24*, 49.
- (6) Tsukahara, Y.; Tanaka, M.; Yamashita, Y. *Polym. J. (Tokyo)* **1987**, *19*, 1121.
- (7) Stejskal, J.; Kratochvíl, P. *J. Appl. Polym. Sci.* **1980**, *25*, 407.

Comparison of Dynamic Rotational Isomeric State Results with Previous Expressions for Local Chain Motion

Ivet Bahar and Burak Erman

School of Engineering, Bogazici University, Bebek, 80815, Istanbul, Turkey

Lucien Monnerie*

Laboratoire de Physicochimie Structurale et Macromoléculaire, associé au CNRS, ESPCI, 10, rue Vauquelin, 75231 Paris, France. Received April 11, 1988

ABSTRACT: The dynamic rotational isomeric states model is used to calculate the conformational (CACF) and first and second orientational (OACF) autocorrelation functions for polyethylene. Various sequence lengths and directions in the chain are considered. The CACFs are compared with Brownian simulation results of Weber and Helfand. Results of calculations on OACFs are analyzed by using the expressions proposed for local chain dynamics by Williams-Watts, Jones-Stockmayer, Bendler-Yaris, and Hall-Helfand. The relationship between the correlation times associated with the first and second OACFs is examined.

Introduction

It is now widely accepted that, among various processes contributing to chain relaxation on a local level, the torsional motion of skeletal bonds, leading to transitions

between isomeric states, plays a dominant role.

A quantitative measure of local orientational motions is the orientational autocorrelation function (OACF), reflecting the transient behavior of one or more vectorial

quantities rigidly embedded in the chain. A large group of experiments investigating local chain dynamics measures either the OACF or its Fourier transform, i.e., the spectral density, associated with specific vectors such as $^{13}\text{C-H}$ bond or H-H internuclear vectors in NMR, the transition moment in fluorescence anisotropy decay, a group of dipole moments in dielectric relaxation, etc. Two types of orientational autocorrelation functions referred to as the first and second OACF's are defined respectively as

$$M_1(t) = \langle \mathbf{m}(0) \cdot \mathbf{m}(t) \rangle \quad (1)$$

$$M_2(t) = \frac{3}{2} \langle (\mathbf{m}(0) \cdot \mathbf{m}(t))^2 \rangle - \frac{1}{2} \quad (2)$$

where \mathbf{m} is the vector whose orientational motion is investigated, the argument denotes the time, and the angular brackets stand for the ensemble average over all possible conformational transitions of the motional sequence to which \mathbf{m} belongs.

In addition to orientational correlation functions, the transient behavior of polymer chains may be described in terms of the conformational autocorrelation functions. The latter refers to the transition probability or conditional probability of occurrence of a given isomeric state at time t for a skeletal bond randomly selected in the chains, given that initially that bond is in the same isomeric state. The time dependence of conformational correlation functions for trans (t) and gauche (g) states for polyethylene (PE) has been obtained through Brownian simulations carried out by Weber and Helfand.¹

In a recently introduced model² describing local chain dynamics, the kinetics and stochastics of conformational transitions were treated in terms of real chain structure and properties. The treatment relies essentially on a model first proposed by Jernigan.³ The equilibrium properties of the polymer chain follow from the usual rotational isomeric states (RIS) model,⁴ i.e., a discrete number of configurations is considered. The model² is accordingly referred to as the dynamic RIS model. It allows for the calculation of both orientational and conformational correlation functions.

In the present study, the decay of the orientational and conformational correlations with time, predicted by the dynamic RIS model, are compared with the expressions proposed by Williams-Watts⁵ (WW), Jones-Stockmayer⁶ (JS), Bendler-Yaris⁷ (BY), and Hall-Helfand⁸ (HH). The expressions proposed by the latter three models contain two parameters reflecting the two essential features of local chain dynamics: (i) the diffusive propagation of orientations along the chain; (ii) the vanishing of the propagation of orientations by various molecular mechanisms.

It should be noted that the expressions of JS and BY have been derived for the second OACF. The HH expression, on the contrary, has been proposed as an extension of the analysis of the first conformational correlation functions to the OACFs. However, the common approach in the literature is to use any of the proposed expressions to interpret experimental results, irrespective of the type of OACF involved. The same attitude is taken in the present study, for the analysis of $M_1(t)$ and $M_2(t)$ obtained by the dynamic RIS model.

A brief outline of the models and the method of calculation is presented in the next section. The results of calculations are given and discussed in the third section.

Models

Dynamic RIS Model. In the dynamic RIS model,² the time-dependent probability of occurrence of isomeric configurations is expressed as a column vector $\mathbf{P}(t)$ obeying the master equation

$$d\mathbf{P}(t)/dt = \mathbf{A} \mathbf{P}(t) \quad (3)$$

where \mathbf{A} is the transition-rate matrix, with negative elements on the diagonal and those in each column summing up to zero, from the principle of detailed balance. For determination of the elements of \mathbf{A} , a suitable kinetic scheme for the passages between conformers must be constructed. The latter necessitates the analysis of N -dimensional conformational maps, for a sequence of N bonds subject to conformational transitions. However, a more convenient approach that has proven to be successful in predicting equilibrium properties is to restrict the analysis to interdependent pairs of adjacent bonds and deduce chain properties from the combination of the results for the pairs. Consequently, eq 3 is initially solved for pairs of bonds. The corresponding rates in \mathbf{A} are represented by Kramers' type expressions that are valid for high-friction Brownian motions, with activation energies obtained from the heights of the saddles in two-dimensional energy maps, in analogy to the kinetic treatment of conformational transitions proposed by Helfand.⁹ A similarity transformation of \mathbf{A} and suitable rearrangements lead to the transition or conditional probability matrix for the pairs, according to²

$$\mathbf{C}^{(2)} = \mathbf{B}^{(2)} \exp\{\mathbf{L}^{(2)}t\}[\mathbf{B}^{(2)}]^{-1} \quad (4)$$

where $\mathbf{L}^{(2)}$ is the diagonal matrix of the eigenvalues of $\mathbf{A}^{(2)}$ and the columns in $\mathbf{B}^{(2)}$ are the corresponding eigenvectors. The superscripts indicate the number of motional bonds.

The conditional probability matrix $\mathbf{C}^{(2)}$ combined with the equilibrium probabilities yields the time-dependent joint probability matrix $\mathbf{P}^{(2)}(t)$ for the pair. Let $p(\alpha\beta, t; \gamma\delta, 0)$ denote the element of $\mathbf{P}^{(2)}(t)$ corresponding to the joint occurrence of states $\alpha\beta$ at time t and $\gamma\delta$ at $t = 0$. Here $\alpha, \beta, \gamma,$ and δ represent the possible isomeric states (t, g⁺, g⁻) that may be assumed by a skeletal bond. For chains with identical skeletal bonds the conditional probability $p(\zeta/\zeta)$ that a bond initially at state ζ , will be at state ζ , at time t as well, is

$$p(\zeta/\zeta) = \frac{\sum_{\alpha} \sum_{\beta} p(\zeta\alpha, t; \zeta\beta, 0)}{p^0(\zeta)} = \frac{\sum_{\alpha} \sum_{\beta} p(\alpha\zeta, t; \beta\zeta, 0)}{p^0(\zeta)} \quad (5)$$

where $p^0(\zeta)$ is the equilibrium probability of state ζ and the summations are performed over all isomeric states for the indicated bond.

Suitable combination² of the elements of $\mathbf{P}^{(2)}(t)$ leads to the time-dependent joint probability matrix $\mathbf{P}^{(N)}(t)$ for N bonds in motion. The latter gives a complete description of the dynamic behavior of the sequence. Accordingly, the OACFs in eq 1 and 2 are computed by using the ij th element $P_{ij}^{(N)}(t)$ of $\mathbf{P}^{(N)}(t)$ in

$$M_1(t) = \sum \sum P_{ij}^{(N)}(t) (\mathbf{m}_i \cdot \mathbf{m}_j) \quad (6)$$

$$M_2(t) = \sum \sum P_{ij}^{(N)}(t) [\frac{3}{2} (\mathbf{m}_i \cdot \mathbf{m}_j)^2 - \frac{1}{2}] \quad (7)$$

Here the subscripts i and j refer to specific configurations of the motional sequence, and the summations are performed over all configurations (3^N of them for N bonds in motion with 3 states available to each). According to the above formulation (eq 6 and 7), all time dependence is accounted for by $P_{ij}(t)$, whereas m_i and m_j are functions of internal configuration only.

Williams-Watts Formulation. This is an empirical expression of the form

$$M_{\text{WW}} = \exp[-(t/\tau)^\beta] \quad (8)$$

The two parameters τ and β may be identified, respec-

tively, as an effective relaxation time and a factor accounting for the deviations from Debye behavior (with $\beta = 1$).

Jones-Stockmayer Model. Both Jones-Stockmayer and Bendler-Yaris theories (see the following subsection) originate from the three-bond motion model first proposed by Valeur and collaborators.¹⁰ The latter, referred to as the VJGM model, uses a continuous limit approximation that leads to an expression with unrealistic infinite slope of the OACF at $t = 0$. Using the same model, Jones and Stockmayer removed this shortcoming by introducing an arbitrary truncation of the coupling of the motion along the chain while keeping the discrete form of the one-dimensional orientational diffusion equation.

In the absence of overall tumbling and Woessner type anisotropic internal rotation, the OACF proposed by Jones and Stockmayer reduces to

$$M_{JS}(t) = \sum G_k \exp(-w\lambda_k t) \quad (9)$$

where λ_k and G_k are found from the sharp cutoff solution of the three-bond jump equation as

$$\lambda_k = 4 \sin^2 [(2k - 1)\pi/4s]$$

$$G_k = 1/s + (2/s) [\sum \exp(-\gamma q) \cos [(2k - 1)\pi q/2s]]$$

where $\gamma = 2 \ln 3$ and $s = (m + 1)/2$. The two adjustable parameters in the theory are w , the characteristic frequency or rate for the three-bond jump model, and m , the number of coupled units at both sides of a central mobile unit. The parameter m ensures the above-mentioned truncation.

Bendler-Yaris Model. An alternate path to the VJGM treatment was proposed by Bendler and Yaris by introducing a short- and a long-wavelength cutoff to the continuous mode spectrum. Thus two correlation times τ_2 and τ_1 characteristic of long- and short-wavelength cutoffs, respectively, are present in the final expression for the OACF as

$$M_{BY}(t) = (\pi/t)^{1/2} [\tau_2^{-1/2} - \tau_1^{-1/2}] [\operatorname{erfc}((t/\tau_1)^{1/2}) - \operatorname{erfc}((t/\tau_2)^{1/2})] \quad (10)$$

Here erfc is the complementary error function.

Hall-Helfand Model. Recently, Hall and Helfand proposed a model for conformational dynamics taking into account correlated pair transitions and isolated transitions occurring at frequencies λ_1 and λ_0 , respectively. The pair transitions ensure the propagation along the chain while the isolated transitions are responsible for the damping. For the simplified case of a one-dimensional chain of two-state elements, they derived the expressions of conformational correlation functions as

$$M_{HH}(t) = \exp(-2\lambda_0 t) \exp(-2\lambda_1 t) I_0(2\lambda_1 t) \quad (11)$$

where I_0 is the modified Bessel function. Although this expression was originally derived as the conformational correlation function, it has proven to fit well both the orientational and conformational decay curves obtained from experiments and Brownian simulations. The recent study by Lin et al.,¹¹ which shows a connection between the JS solution to the three-bond jump equation and the HH expression, supports the use of the latter for describing OACFs.

Results of Calculations and Discussion

Conformational Autocorrelation Functions (CACF). The conditional probability $p(\zeta/\zeta)$ of occurrence of a given isomeric state for a bond at time t , given the identical initial state, is calculated according to eq 5 in the dynamic RIS model. Calculations are performed for

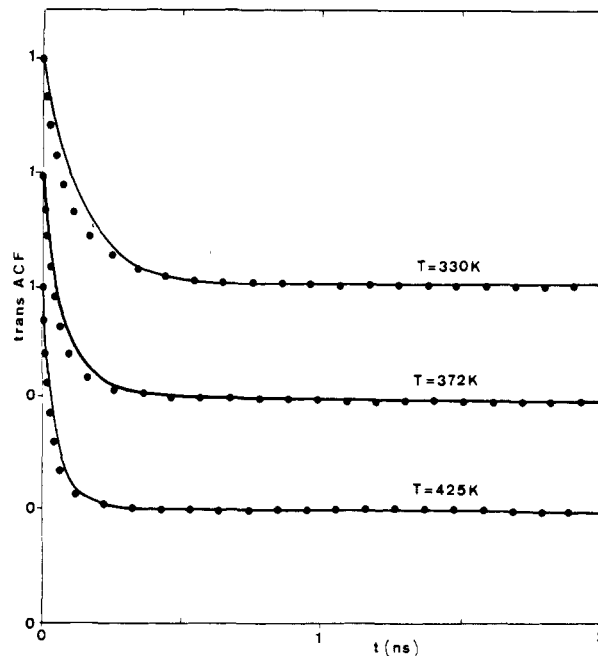


Figure 1. Comparison of the conformational autocorrelation functions from the dynamic RIS calculations (curves) with results of Brownian simulations (filled circles) of Weber and Helfand, for polyethylene at three different temperatures. The ordinate represents the autocorrelation function for the trans state.

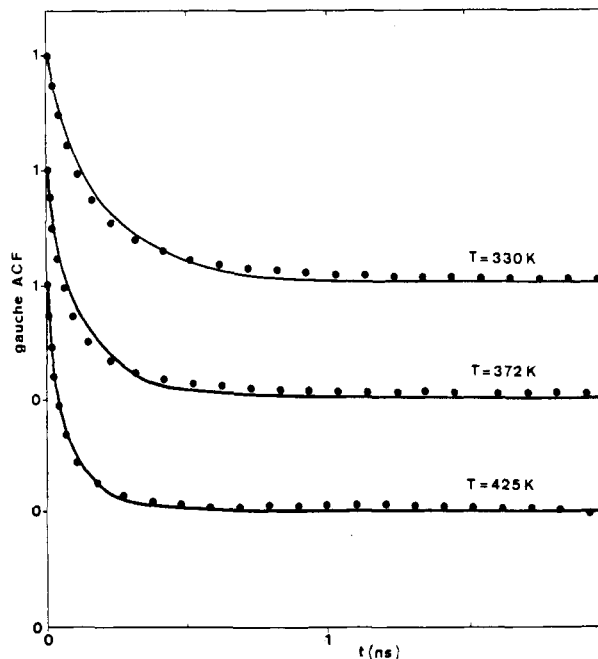


Figure 2. Autocorrelation function for the gauche state of a bond in polyethylene. See legend to Figure 1.

polyethylene, for the trans and gauche states. Thus ζ is replaced by t and g , respectively. In the limit as time $\rightarrow \infty$, $p(t/t)$ and $p(g/g)$ will be converging to the equilibrium probabilities of the trans and gauche states, respectively. The conditional probabilities are properly normalized to ensure the decay to zero, in accordance with the similar approach by Weber and Helfand.¹ The resulting (CACF) curves for $T = 330, 372,$ and 425 K are shown in Figures 1 and 2. The curves have been obtained by using the same energy parameters and preexponential factor ($2.77 \times 10^{11}/s$) as those previously adopted.^{2,12,13} The filled circles represent results from Brownian simulations carried out by Weber and Helfand. It should be noted that interdependence between second neighbors along the backbone

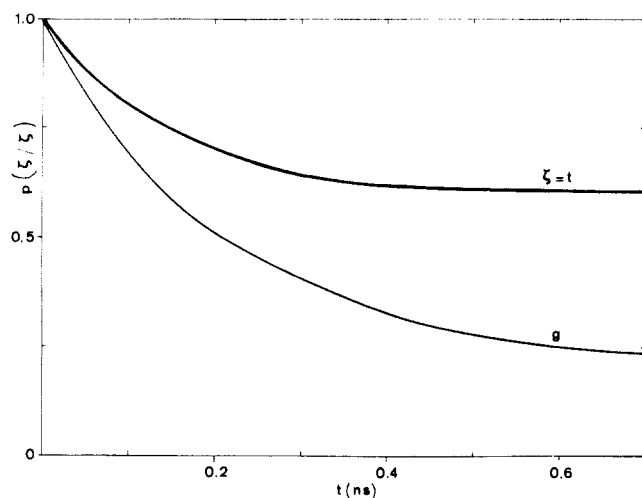


Figure 3. Conditional probability $p(\xi/\xi)$ that a bond is in state ξ both at time 0 and t . Calculations are for polyethylene at 330 K.

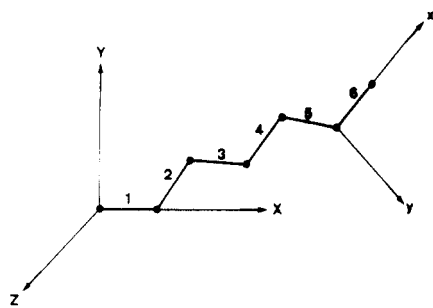


Figure 4. Sequence of six bonds with four bonds in motion. The first two bonds are fixed in the XY plane of a fixed reference frame $OXYZ$. The x and y axes of the sixth bond based frame is also shown. The y axis is chosen to make an acute angle with the fifth bond. The z axis is normal to the plane of bonds 5 and 6.

(counter rotations, etc.), which is pointed out to play a major role in local chain dynamics, is not directly considered in the present computation scheme. Also the parameters adopted in Brownian simulations are somewhat different from those used in the present dynamic RIS model. The latter neglects the deformation of bond lengths and bond angles and limits the analysis to the torsional motion of skeletal bonds, which is asserted to be the dominating mechanism for chain relaxation. In view of the several approximations in the two approaches, the agreement between the dynamic RIS model and the Brownian simulations may be considered as rather satisfactory.

Comparison of the decay of the gauche and trans ACFs from the normalized curves in Figures 1 and 2 is somehow misleading. Indeed, the apparent decay rate for the gauche state is slower than that of the trans state. In reality, from the principle of detailed balance, states with lower equilibrium probabilities (gauche in the present case of PE), will exhibit a stronger tendency to change their state, i.e., their transition rate will be higher. The correct comparison of the behavior of the t and g states has to be carried out before normalization of the CACFs. This is shown in Figure 3, where the expected more rapid decay of $p(g/g)$ is clearly seen.

Orientational Autocorrelation Functions. The decay of the first and second OACFs with time for PE is computed according to the dynamic RIS model, with eq 6 and 7, respectively. Calculations are performed for the three vectors spanning the n th bond-based frame (Figure 4) of a series of sequences in motion varying in length. The

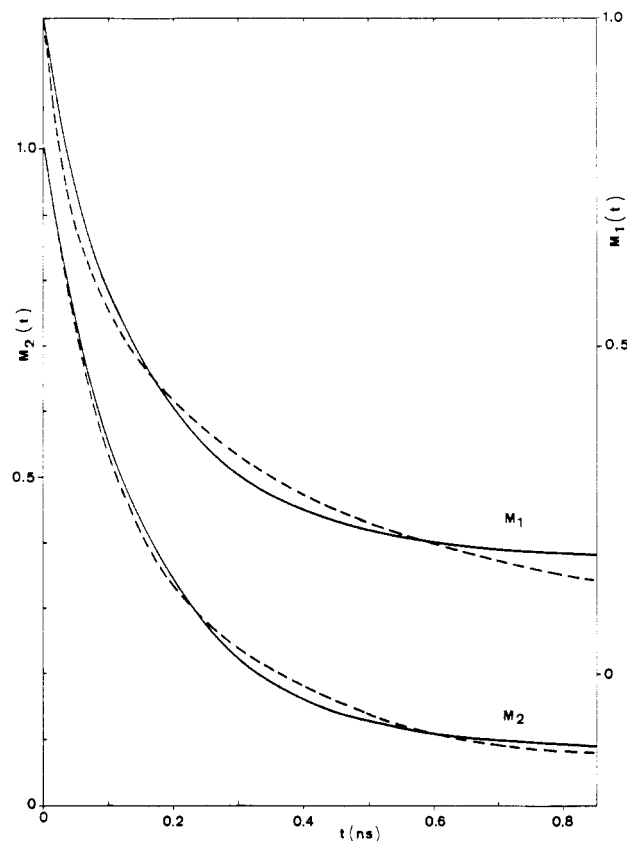


Figure 5. Comparison of the dynamic RIS calculations (solid curves) for $M_1(t)$ and $M_2(t)$ with results of the WW expression (dashed curves). Calculations are for $n = 6$, $T = 300$ K for a vector along the bond axis.

first two bonds of the sequence are held fixed in a laboratory-fixed coordinate system while the others are free to assume any orientation compatible with the local configurational stochastics of the specific chain. The resulting autocorrelation curves are analyzed in comparison to the four expressions given by eq 8–11. The two parameters in each expression are optimized to yield the decay curves that best approximate the OACFs resulting from the dynamic RIS model. The procedure is based upon determination of the pair of parameters that minimizes the mean-square deviation χ^2 . The latter is defined as

$$\chi^2 = \sum \{ [M(t_i) - M_{XX}(t_i)]^2 / M(t_i) \} \quad (12)$$

where M_{XX} denotes the OACF calculated from model XX (i.e., WW, JS, BY, HH), $M(t_i)$ refers to $M_1(t)$ and/or $M_2(t)$ calculated at time t_i , by the dynamic RIS model.

It should be noted that in the dynamic RIS model correlations between successive bonds are taken into account in such a way that only the intramolecular contributions to relaxation are included. As a result, the calculated OACFs do not go to zero as $t \rightarrow \infty$ but go to an asymptotic value. In the real situation, the tumbling of the overall molecule or large portions of the molecule takes place and leads to further relaxation at long times; consequently the real OACF decays to zero. Within the time scale of 0–0.8 ns, the effect of tumbling is negligible if we assume for example $\tau_0 = 10^{-8}$ – 10^{-7} s, where τ_0 is the correlation time for overall tumbling. In fact, the overall tumbling is dominant for low-molecular-weight compounds, but as the molecular weight increases local motions take precedence, as pointed out by Matsuo and collaborators¹⁴ on the basis of NMR experiments where the time scale is of the order of 10^{-10} s, as in the present study. The absence of overall tumbling is therefore of no significant

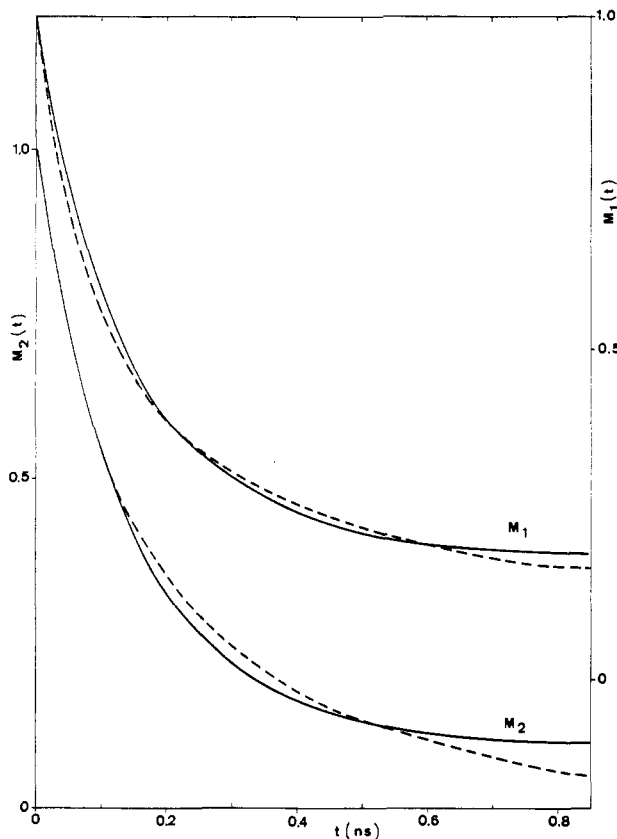


Figure 6. Comparison of the dynamic RIS calculations (solid curves) for $M_1(t)$ and $M_2(t)$ with results of the JS model (dashed curves). Calculations are for $n = 6$, $T = 300$ K for a vector along the bond axis.

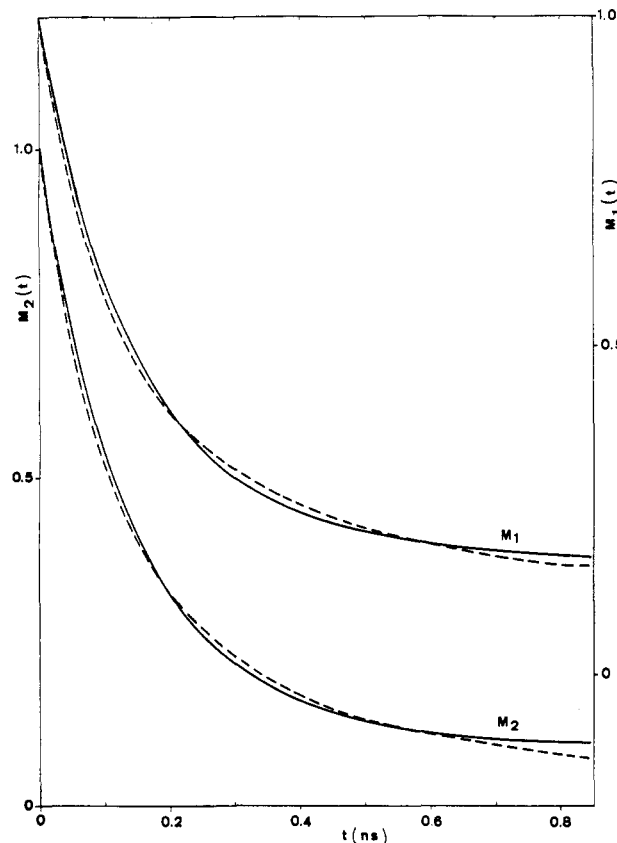


Figure 7. Comparison of the dynamic RIS calculations (solid curves) for $M_1(t)$ and $M_2(t)$ with results of the BY model (dashed curves). Calculations are for $n = 6$, $T = 300$ K for a vector along the bond axis.

consequence in the interval 0–0.8 ns. We accordingly restrict our comparison to this time interval in the following.

Figures 5–9 depict the OACF curves calculated by the dynamic RIS model for the sixth bond ($n = 6$) from a fixed origin in PE, and those obtained with the parameters minimizing χ^2 for each functional form (i.e., eq 8–11). Solid curves follow from the dynamic RIS model. Dashed curves are obtained by using the best-fitting parameters in WW (Figure 5), JS (Figure 6), BY (Figure 7), and HH (Figures 8 and 9) expression. In Figures 5–7, the vertical axes on the right and on the left correspond to the first and second OACFs for the x -component, respectively. Curves in Figures 8 and 9 represent the OACFs associated with the x , y , and z directions in bond-based coordinate systems, as shown in Figure 4.

A list of the best-fitting parameters and corresponding χ^2 is presented in Table I. Results are tabulated for $n = 6$ and 8 and unit vectors along x , y , and z directions. The reported χ^2 values are obtained from eq 12, with t_i (ns) = $0.05i$, where i takes the values from 1 to 16.

From the analysis of the curves in Figures 5–9 and Table I, it may be observed that the OACFs obtained by the dynamic RIS model may be approximated to a certain extent by all of the four expressions considered. Best fits are achieved with HH and BY expressions.

The decay of the OACFs with time cannot be represented by single exponentials, as is well established from a large number of experimental and theoretical studies. In fact an exponent β , different from unity, is definitely required to minimize χ^2 when the Williams–Watts expression is used. Also there is a need for the introduction of a damping parameter, regardless of the model selected except for $M_1(t)$ of bond vectors for $n \leq 6$, where the parameters $1/\lambda_0$ and τ_2 in HH and BY models, respec-

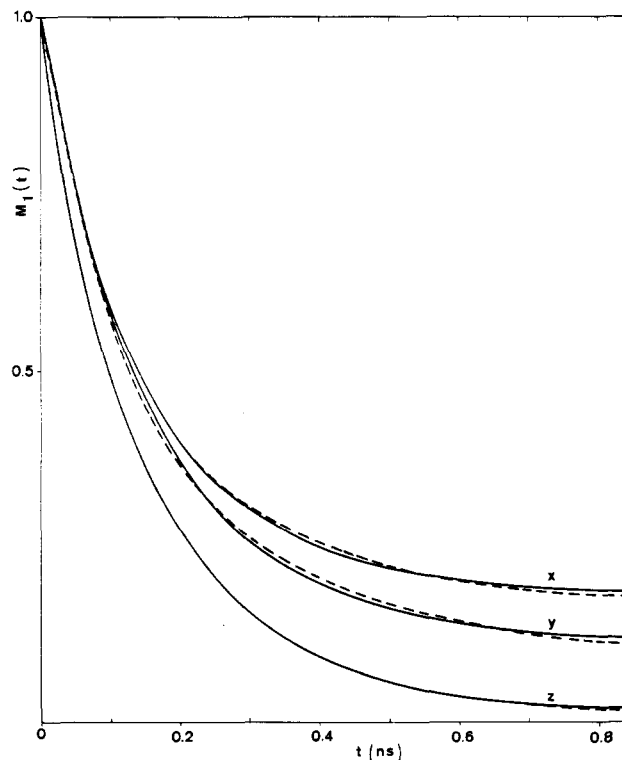


Figure 8. Comparison of the dynamic RIS calculations (solid curves) for $M_1(t)$ with results of the HH model (dashed curves). Calculations are for $n = 6$, $T = 300$ K for three directions along x , y , z axes of the bond-based frame.

tively, are relatively large (for $n = 5$, $1/\lambda_0 = 500$ ns and $\tau_2 = 22$ ns). In this particular case, the OACF may be reproduced to a good approximation by neglecting the

Table I

			WW			JS			BY			HH		
			β	τ , ns	χ^2	m	$1/w$, ns	χ^2	τ_2 , ns	τ_1 , ns	χ^2	$1/\lambda_0$, ns	$1/\lambda_1$, ns	χ^2
M_1	x	6	0.56	0.255	0.043	5	0.240	0.016	10	0.050	0.011	10	0.16	0.0045
		8	0.53	0.125	0.070	5	0.122	0.062	2.0	0.032	0.031	1.4	0.10	0.022
		8	0.64	0.21	0.037	3	0.240	0.041	2.0	0.059	0.013	1.4	0.17	0.008
y	6	0.60	0.12	0.059	3	0.156	0.106	1.0	0.037	0.026	0.72	0.11	0.027	
	8	0.84	0.15	0.007	3	0.140	0.047	0.39	0.071	0.003	0.34	0.21	0.005	
	8	0.84	0.105	0.019	3	0.101	0.043	0.27	0.050	0.010	0.24	0.16	0.005	
M_2	x	6	0.64	0.18	0.046	3	0.208	0.061	1.43	0.056	0.015	1.03	0.15	0.017
		8	0.66	0.10	0.056	3	0.120	0.097	0.59	0.033	0.032	0.45	0.095	0.028
		6	0.63	0.20	0.042	3	0.241	0.005	2.0	0.055	0.014	1.47	0.16	0.011
y	8	0.63	0.11	0.065	3	0.135	0.096	1.0	0.037	0.026	0.56	0.10	0.025	
	6	0.89	0.13	0.006	3	0.119	0.073	0.27	0.077	0.004	0.25	0.25	0.003	
	8	0.91	0.10	0.008	3	0.083	0.033	0.385	0.056	0.002	0.19	0.145	0.007	

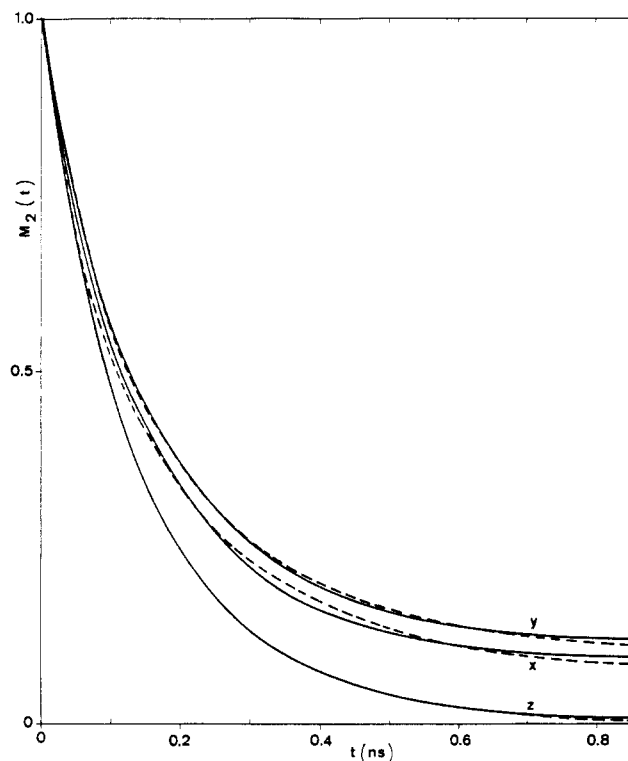


Figure 9. Comparison of the dynamic RIS calculations (solid curves) for $M_2(t)$ with results of the HH model (dashed curves). Calculations are for $n = 6$, for three directions along x , y , z axes of the bond-based frame.

contribution of τ_2 or $1/\lambda_0$ to relaxation, i.e., setting them equal to infinity. However, calculations indicate that as n increases, finite $1/\lambda_0$ or τ_2 values are required to achieve best curve fittings.

Comparison of the best-fitting parameters from various models shows that the time parameter τ in WW and $1/w$ in JS are very close to each other for both OACFs in all directions, while the damping parameters τ_2 and $1/\lambda_0$ in BY and HH, respectively, are of comparable magnitude. On the other hand, the parameter $1/\lambda_0$ accounting for the damping of the motion is at least 1 order of magnitude larger than $1/\lambda_1$, in agreement with previous curve-fitting calculations carried out by Helfand et al. to reproduce the decay of the OACFs resulting from their Brownian simulations.

It has been recently shown¹² that the decay of the first and second OACFs occur within about the same time range. Let $M_{1v}(t)$ and $M_{2v}(t)$ represent the OACFs for $\mathbf{v} = \mathbf{x}$, \mathbf{y} , or \mathbf{z} , i.e., the unit vectors along the coordinates of the local frame investigated. It has been pointed out¹² that $M_{2y}(t)$ decays slower than $M_{2x}(t)$ for PE while relative behavior of the corresponding first OACFs is inverted. The

Table II

θ	$\theta(M_1)/\theta(M_2)$					
	x		y		z	
	$n = 6$	$n = 8$	$n = 6$	$n = 8$	$n = 6$	$n = 8$
τ (WW)	1.42	1.25	1.05	1.09	1.15	1.05
λ_1^{-1} (HH)	1.07	1.05	1.06	1.10	0.84	1.10
$1/w$ (JS)	1.15	1.02	1.00	1.16	1.18	1.22
τ_1 (BY)	1.00	0.97	1.07	1.00	0.92	0.89

Table III
Comparison of θ' Values from Various Models

θ'	$n = 8$					
	x		y		z	
	$\theta'(M_1)$	$\theta'(M_2)$	$\theta'(M_1)$	$\theta'(M_2)$	$\theta'(M_1)$	$\theta'(M_2)$
τ (WW)	0.55	0.65	0.62	0.63	0.84	0.90
$1/\lambda_0$, ns (HH)	1.40	0.45	0.72	0.56	0.24	0.16
m (JS)	3	5	3	3	3	3
τ_2 , ns (BY)	10.0	1.43	2.0	2.0	0.39	0.27

present analysis provides an opportunity to compare $M_{1v}(t)$ and $M_{2v}(t)$ on more quantitative grounds.

For isotropic motion, the correlation times associated with $M_{1v}(t)$ are 3 times as large as those from $M_{2v}(t)$. In the case of the models derived for the dynamic behavior of the polymeric chains, the relationship between the correlation times associated with $M_{1v}(t)$ and $M_{2v}(t)$ is unknown. The dynamic RIS calculations give an insight into this question. Let us first consider the correlation times related to the conformational changes propagating along the chain. We have listed in Table II the ratio of these correlation times $\theta(M_1)$ and $\theta(M_2)$ associated with $M_{1v}(t)$ and $M_{2v}(t)$, respectively, for $n = 6$ and 8, obtained from the fitting with the various models (Table I). It may be observed from the tabulated values that $\theta(M_1)$ exceeds $\theta(M_2)$ by about 10%, in general, regardless of the direction of the investigated vector with respect to the backbone.

As to the parameters that reflect the damping or localization of the motion, their numerical values are often quite different for $M_{1v}(t)$ and $M_{2v}(t)$. For this reason, we have listed in Table III the respective values $\theta'(M_1)$ and $\theta'(M_2)$ obtained for $n = 8$ from the fitting with the various models. It is found that θ' values relative to the bond vectors \mathbf{x} differ considerably for $M_{1x}(t)$ and $M_{2x}(t)$, while values for vectors in the y and z directions are almost constant.

To examine the effect of the sequence lengths on the OACFs, we have limited our analysis to the fitting parameters of the HH expression for the bond vector \mathbf{x} . A first analysis carried out over the time range 0–0.9 ns has shown significant decrease in the correlation times with increasing n . In the interest of performing a consistent analysis for each value of n , the fitting has been performed over a time interval corresponding to about 98% of full

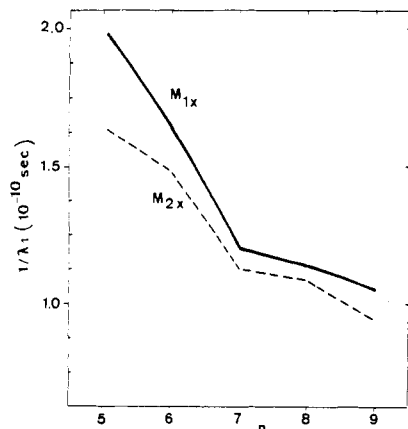


Figure 10. Dependence of the best fitting λ_1 from HH expression on sequence length for M_1 (solid line) and M_2 (dashed line).

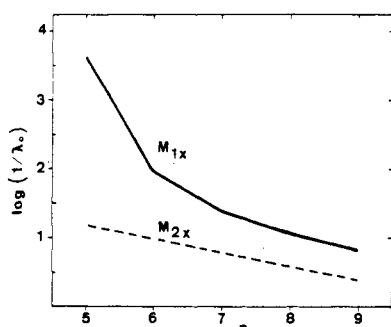


Figure 11. Dependence of the best fitting λ_0 from HH expression on sequence length for M_1 (solid line) and M_2 (dashed line). Units of λ_0 are 10^{-10} s^{-1} .

relaxation. Figure 10 depicts the change in $1/\lambda_1$ with n for the first (solid line) and second (dashed line) OACFs. As mentioned above, the increase in chain length leads to an increase of the frequency of the motion, due to larger number of available paths to relaxation, in agreement with previous studies.^{2,12,13} The curves in Figure 10 allow to some extent estimation of suitable parameters for longer sequences. In fact, sequences varying in length are expected to contribute to chain relaxation, and a rigorous analysis necessitates the knowledge of the dynamic behavior of longer sequences, as well. The latter, however, will be increasingly influenced by environmental constraints, and consequently parameters deduced from Figure 10 through extrapolation must be considered with some caution.

For convenience, the logarithm of the parameter λ_0 associated with the damping of the diffusion, is plotted

against n , in Figure 11, for the first (solid line) and the second (dashed line) OACFs. The apparent effect of an increase in n is a substantial decrease in the correlation time $1/\lambda_0$.

Conclusion

The results reported in this work first demonstrate that in spite of the limited lengths of the sequences considered in the dynamic RIS calculations the resulting CACFs agree satisfactorily with those obtained by Brownian simulation on a ring chain with 200 bonds. Second, the calculated OACFs can be well fitted by the previously proposed Bendler-Yaris and Hall-Helfand expressions. Furthermore, it appears that for a polymer chain, the two correlation times, characteristic of the conformational changes, associated with the first and second OACFs are very close to each other. This feature is in strong contrast to that for isotropic motion (the Debye model) where the correlation times differ by a factor of 3.¹⁵ This follows from the fact that rotational reorientations are of the jump-diffusion type where the vector of interest reorients by a series of discontinuous jumps, resulting from rapid excursions of bonds between rotational isomeric states. This is in contrast with the Debye model, which is based on infinitesimal jumps according to which distribution of jump angles are highly peaked for small angles and $\tau_2/\tau_1 = 1/3$.

Acknowledgment. This work was supported by NATO Grant No. 0321/87.

Registry No. Polyethylene, 9002-88-4.

References and Notes

- (1) Weber, T. A.; Helfand, E. *J. Phys. Chem.* **1983**, *87*, 2881.
- (2) Bahar, I.; Erman, B. *Macromolecules* **1987**, *20*, 1368.
- (3) Jernigan, R. L. In *Dielectric Properties of Polymers*; Karasz, F. E., Ed.; Plenum: New York, 1972; p 99.
- (4) Flory, P. J. *Statistical Mechanics of Chain Molecules*; Wiley Interscience: New York, 1969.
- (5) Williams, G.; Watts, D. C. *Trans. Faraday Soc.* **1971**, *66*, 80.
- (6) Jones, A. A.; Stockmayer, W. H. *J. Polym. Sci., Polym. Phys. Ed.* **1977**, *15*, 847.
- (7) Bendler, J. T.; Yaris, R. *Macromolecules* **1978**, *11*, 650.
- (8) Hall, C. K.; Helfand, E. *J. Chem. Phys.* **1982**, *77*, 3275.
- (9) Helfand, E. *J. Chem. Phys.* **1971**, *54*, 4651.
- (10) Valeur, B.; Jarry, J. P.; Gény, F.; Monnerie, L. *J. Polym. Sci., Polym. Phys. Ed.* **1975**, *13*, 667, 675, 2251.
- (11) Lin, Y. Y.; Jones, A. A.; Stockmayer, W. H. *J. Polym. Sci., Polym. Phys. Ed.* **1984**, *22*, 2195.
- (12) Bahar, I.; Erman, B. *Macromolecules* **1987**, *20*, 2310.
- (13) Bahar, I.; Erman, B. *J. Chem. Phys.* **1988**, *88*, 1228.
- (14) Matsuo, K.; Kuhlmann, K. F.; Yang, H. W.-H.; Gény, F.; Stockmayer, W. H.; Jones, A. A. *J. Polym. Sci., Polym. Phys. Ed.* **1977**, *15*, 1347.
- (15) Berne, B. J.; Pecora, R. *Dynamic Light Scattering*; Wiley-Interscience: New York, 1976.